

Metalenses at visible wavelengths: past, present, perspectives

Authors: Philippe Lalanne^{1*}, Pierre Chavel^{2*}

Affiliations:

¹ Laboratoire Photonique, Numérique et Nanosciences (LP2N), IOGS – Univ. Bordeaux – CNRS, 33400 Talence cedex, France.

² Laboratoire Charles Fabry (LCF), IOGS – CNRS – Univ. Paris-Saclay, 2 avenue Augustin Fresnel, 91127 Palaiseau cedex, France.

*Correspondence to: philippe.lalanne@institutoptique.fr, pierre.chavel@institutoptique.fr

Abstract: The so-called ‘flat optics’ that shapes the phase of an incident wave in free space through subwavelength structures has a venerable history. In that domain, achieving high efficiency at large deflection angles requires a low absorption material, a suitable technological process, as well as a guiding effect in the nanostructures.

1. Introduction

Since the publication of a research article in *Science* that revisited Snell’s law at the interface between two uniform media thanks to an ultrathin metallic grating etched on the interface [Yu11], metasurfaces and especially metalenses, are the subject of an intense research activity, leading to numerous publications in high-impact journals and great promises. A recent research article [Kho16] that reports metalenses manufactured with a high numerical aperture (NA) operating at visible wavelengths is particularly emblematic of this growing interest. Comparisons with a state-of-the-art commercial objective suggest that the image quality is as good and even better, and considering their flat nature and compact size, metalenses appear as potentially revolutionary. However, metalenses do not come out of the blue and the so-called ‘flat optics’ that shapes the phase of free-space waves through subwavelength structures have a venerable history over many years from the microwave domain down to the visible. What is the paradigm change at the source of this anticipated revolution? New fabrication processes, new concepts, new applications, fundamental limitation shifts?

To answer these questions, we confront recent metalens achievements with an historical perspective of flat optical elements, to further analyze the fundamental limitations that have been lifted and better anticipate perspectives offered by flat optics. This is precisely the outline of the present article, which starts with a brief overview of the fundamentals of flat optics.

2. Flat-optic basis

The basic role of optical components such as lenses or prisms is to shape incoming wavefronts. In recent years, various flat-optics components with an optical thickness on the order of the wavelength have been introduced and demonstrated. In contrast to bulk optics, where phase is modulated by a continuous variation of the optical thickness, flat optics restrict the modulation to its minimum, 2π , by wrapping the bulk-optics phase modulo 2π for a nominal design wavelength λ . The wavefront is divided into zones wherein the phase varies by 2π , with a 2π discontinuity between them. At λ , the diffraction patterns of the various zones combine coherently to form exactly the initial continuous wave, if the zone widths are much larger than λ . At other wavelengths, the wrapping procedure introduces a specific dispersion effect that splits the wavefront into a set orders and therefore reduces the diffraction

efficiency of the desired order [Swa89]. Compared to travelling the same distance in air (of index assumed to be unity), the optical path delay for a zone thickness t is

$$\Delta = (n - 1)t. \quad [1]$$

Conventional diffractive optical components [Aur72], such as the well-known “échelette” blazed grating, implement a 2π -phase delay across the component surface by a $\lambda/(n - 1)$ thickness excursion of the diffractive surface profile.

Nowadays, échelette-type diffractive optical elements are manufactured at low-cost with replication technologies such as embossing, moulding and casting. The latter offer very high resolution, typically in the nanometer range, and allow the fabrication of large area, complex microstructures with minimal light loss in durable materials through high volume industrial production processes [Gal97]. They have however two fundamental limitations:

- The discontinuities of the wrapped phase introduce a shadow that wastes light into spurious orders. The effect is stringent for short échelettes, to an extent that the échelette approach is essentially useless for high-NA lenses.
- The wrapping relies on a nominal design wavelength λ , implying that the imprinted phase varies with the wavelength of the incident light. Thus, the efficiency decreases as the illumination wavelength departs from the nominal one.

Alternatively, here we consider components for which the index spans an excursion of λ/t by patterning the material at a subwavelength scale to tailor the “effective index” experienced by the transmitted wavefront, with a view to understand if they can lift the fundamental limitations of échelettes. In recent years, the name “metasurfaces”, arising from the field of plasmonics, has been used to designate the graded index components. Because they encompass a new type of blazed components derived from binary masking, they were also called “blazed binary” components or “artificial distributed-index” components in earlier times.

3. Metalens: an historical fresco

While the concept of an effective index can be traced back to over hundred years, it was apparently not applied to wavefront shaping until the time of Kock [Koc48], who fabricated microwave diffractive lenses in high-index artificial dielectrics obtained by doping polystyrene foam sheets with subwavelength metallic inserts. Drastic weight reduction was achieved with half-wavelength resonant inserts, but broader frequency operation was achieved with slightly smaller inserts.

Extension to shorter wavelengths, did not occur until much more recently. Researchers in Erlangen [Sto91] and at MIT [Far92] were the first to propose monitoring the phase of graded-index materials in the infrared, and then in the visible domain. The first experimental demonstrations of reflection gratings and a cylindrical mirror were performed at $\lambda = 10.6 \mu\text{m}$ with metallic grooves of graded widths [Kip94].

Initial demonstrations of blazed-binary components manufactured at visible frequencies by etching quartz, glass and polymer films were disappointing, with measured diffraction efficiencies smaller than those of échelette components [Che95, Zho95, Mil96, Che96, War96]. At that time, the design mostly assumed an “adiabatic” index gradient, the analogy between local subwavelength gratings and artificial dielectrics was not properly understood, and modeling was challenging. Most importantly, the combined requirements of subwavelength spacing and 2π -phase excursion led to aspect ratios difficult to manufacture with the materials and patterning technologies implemented.

New perspectives opened up by manufacturing blazed-binary components in high-index materials. For operation in the visible, TiO_2 appeared to be the most suitable transparent material. Figure 1 summarizes the main results in [Lal98,Lal99], which were obtained for a series of gratings with increasing deviation angle for operation with an HeNe laser emitting at $\lambda = 633 \text{ nm}$. The smallest pillar width is 90 nm, and the pillar spacing used to sample the phase is 272 nm. The gratings were fabricated by direct e-beam writing, liftoff and chemically-assisted reactive ion etching using a process detailed in [Lal98]. Remarkably, efficiencies surpassing the hegemonic échelette components were observed for highly dispersive gratings corresponding to large deviation angles. The same concept applies to lenses: for the first time, one could therefore envision to implement efficient lenses with high- NA , removing of the two main limitations of échelette diffractive lenses.

Indeed, that demonstration was immediately followed by the fabrication of a 20° off-axis lens operating at $\lambda = 850 \text{ nm}$ with a vertical-cavity-surface-emitting laser for possible application to optical interconnects, see the SEM picture shown in Fig. 2c. The lens had an NA of 0.25 but since it was designed for a 20° off-axis operation, the Fresnel zone widths were all smaller than 9λ . Half of the aperture was composed of zones with widths smaller than 3λ , corresponding to a much larger NA for an on-axis lens. Even so, the measured efficiency, including Fresnel reflections, reaches an impressive 80% [Lal99].

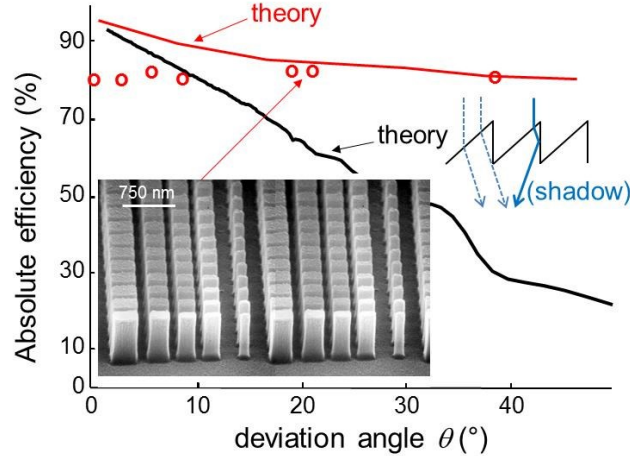


Fig. 1. Blazed binary diffractive elements beat their échelette counterparts with respect to the efficiency. First-order transmission efficiencies of blazed-binary gratings as a function of the deviation angle θ in air (the grating period is varying) for a normally-incident and unpolarized plane wave at $\lambda = 633 \text{ nm}$. Circles: experimental results. Red curve: theoretical results. The discrepancy at small θ is due to over etching fabrication errors resulting in a bond failure of tiny pillars. Black curve: theoretical results for échelette gratings in glass. The lower inset is an electron micrograph of a section of the grating operating at $\theta = 20^\circ$; the period is $1.9 \mu\text{m}$, the pillar aspect ratio reaches 4.6. The right inset shows the shadow zone responsible for efficiency drop of échelette gratings at large θ 's. After [Lal98,Lal99,Lee02].

It is appropriate to underline why the échelette efficiencies were surpassed. For large deviation angles, the prism angle in each échelette period is as large as to cast shadow on the neighbors, wasting light into spurious orders, as illustrated in the right-hand side inset of Fig. 1 for normal incidence. The effect worsens at large deviation angle and at oblique incidence, as the relative impact of the shadow

zone on the diffraction increases. In contrast, for high-index blazed-binary diffractive elements, every pillar behaves as an independent monomode waveguide that confines the light throughout the structure. No shadowing effect occurs even for oblique incidence [Lee02] with the small diffraction zones of high-NA components. In fact, such components operate at the limit of validity of the effective-index concept and behave analogously to phased arrays in radars [La99a]. Among other recent implementations, the most remarkable application of such components to date might be the Gaia grating [Zei10] sent to space in 2013 (period 3.15 μm , efficiency >80% over a 20.5 x 15.5 cm area).

The subject of metalenses has received considerably renewed attention recently with the introduction of resonance effects for monitoring the phase. Because resonance amplifies the phase delay compared to the propagation delay of Eq. [1], the requirement for large aspect ratios is relaxed.

Plasmonic-based metasurfaces composed of tiny metallic nanoantennas were initially considered [Yu11]. Two approaches were developed to achieve the required 2π -phase excursion. The first relies on the generation of two resonances, which can be independently tuned, each covering a standard phase range of π . For example, V-shaped antennas with different arm lengths and angles can generate symmetric and asymmetric modes. Full wavefront control can be achieved by varying the geometry of the antennas. The second approach is based on rotationally asymmetric nanostructures whose resonant modes are polarization dependent. Complete phase control can be achieved by spatially varying the geometric orientation of the nanostructures [Hua13]. However, Ohmic losses in the metal have limited high efficiencies to reflection mode operation only [Che14].

Whence the recent revival of interest for dielectrics metalenses. One of the newly introduced options is to replace the nanoantennas by high-index dielectric subwavelength microresonators showing form birefringence. By rotating the microresonators, a vortex is created and a fancy mutual polarization behavior for right-handed and left-handed input-output beams arises [Lin14, Kho16]. Another option, which is polarization insensitive like the blazed-binary components developed in the 90's, uses micropillars that support two propagating modes in either polarization [Vo14, Arb15, Yu15]. The 2π -phase excursion is then implemented with a combination of two resonances with relaxed aspect ratios.

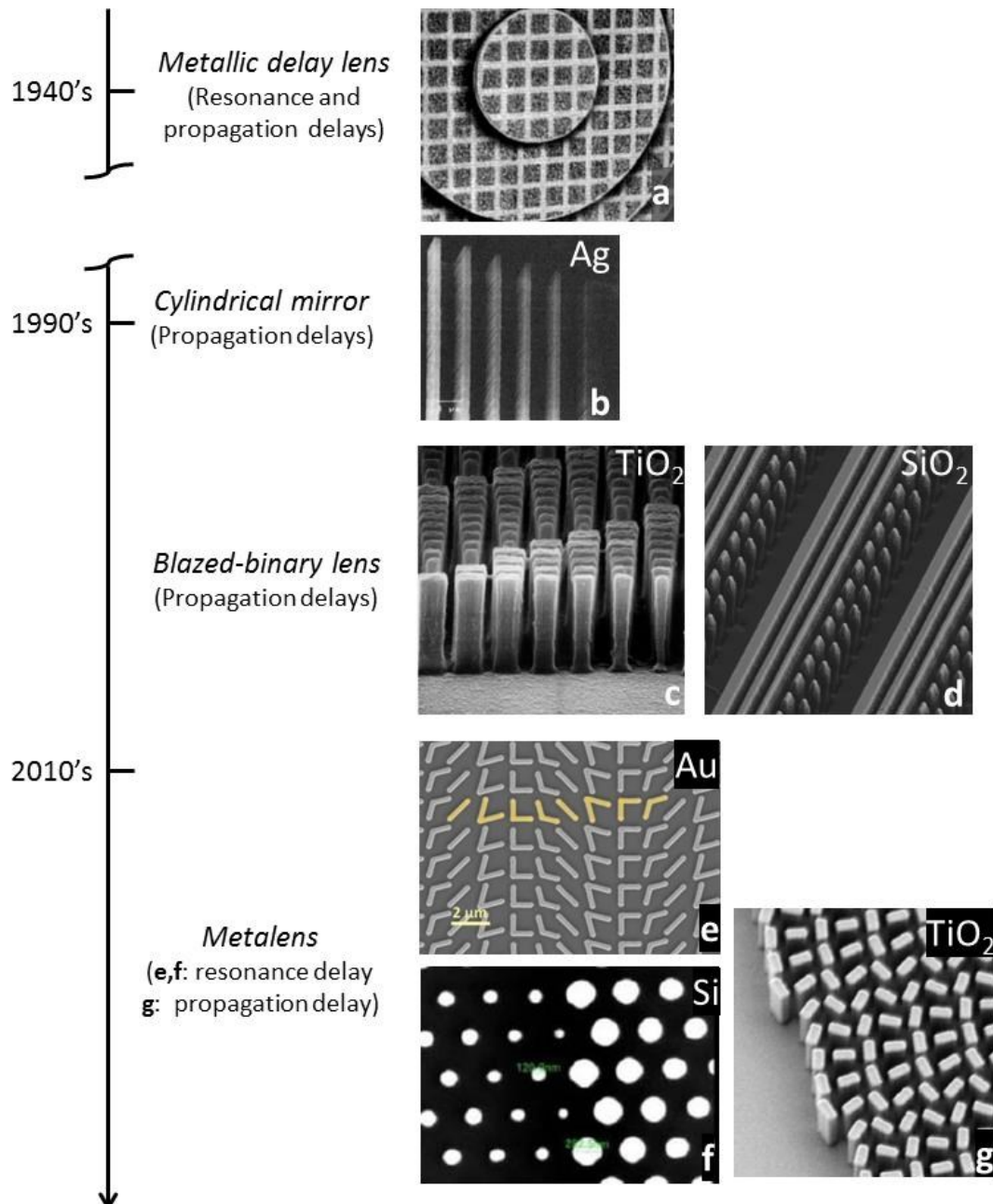
By way of summary, Fig. 2 provides an historical overview of the concepts used so far for designing and fabricating flat optical wavefront shapers based on subwavelength binary nanostructures.

4. Limitations and perspectives

4.1 Design constraints

The art of dielectric metalens design is to devise recipes to imprint the wrapped phase on a surface with a high fidelity, minimizing potential spurious effects introduced by the discontinuities. The design of diffractive lens with subwavelength dielectric pillars faces two conflicting perspectives.

On one side, one would prefer to have small spacing between pillars (right panel in Fig. 3). Then, the phase would be finely sampled, which might be important especially for the outer zones of high-NA lenses. However, in addition to fabrication issues, there is a lower bound for the spacing. Indeed one expects that every pillar be electromagnetically independent from its neighbors [La99a, Lee02]. This condition is fundamental as it guarantees that 1/ high efficiency is achieved by lowering the shadow effect and 2/ the imprinted phase is independent of the parallel wavevector of the incident beam, implying that the same pillar structure can be used for a broad range of incidence angles and may effectively either focus any obliquely incident plane wave, or collimate any diverging beam, as shown by the off-axis lens reported in [Lal99]. Large nanopillar spacings, decoupling the evanescent tails of the pillar modes, are thus preferred (central panel in Fig. 3).



Reference	Efficiency	mode	material	λ	polarization	t/λ
a: [Koc48]	not reported	T	composite	7 cm	insensitive	not reported
b: [Kip94]	80%	R	Ag	10.6 μ m	linear	0.7
c: [Lal99]	80%	T	TiO ₂	633-850 nm	insensitive	1.15
d: [Zei10]	>80%	T	SiO ₂	850 nm	insensitive	2.1
e: [Yu11]	weak	T	Au	8 μ m	linear (cross)	0.006
f: [Vo14]	70%	T	Si	850 nm	insensitive	0.56
g: [Kho16]	66-86%	T	TiO ₂	405-660 nm	circular (cross)	0.9

Fig. 2. Historical fresco of wavefront shaping with metasurfaces. R and T mean reflection and transmission mode operation, respectively, and “cross” refers to incident and diffracted beams which are mutually cross-polarized.

On the other side, to accurately imprint the wrapped phase, a monomode propagation is required for light transfer through the diffractive surface. This requires that the pillar spacing be smaller than an upper bound, called the structural cutoff in [Lal99], which guarantees that a single supermode per polarization propagates in the pillar array (left panel in Fig. 3), all the other supermodes being evanescent.

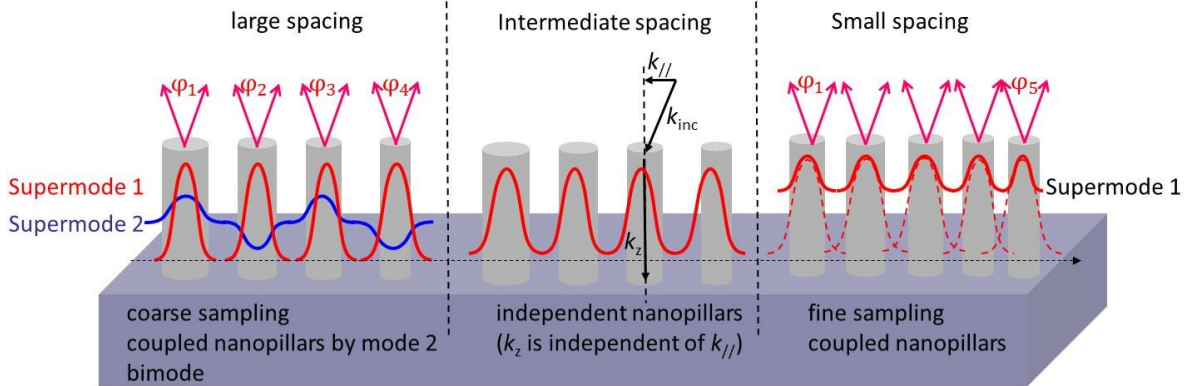


Fig. 3. Optical phase arrays. Right panel: small spacings. The phase sampling is fine, the nanopillars are coupled electromagnetically and the supermode propagation constant k_z varies with the parallel wavevector k_{\parallel} of the incident plane wave. The shadow zone is not completely eliminated. Central panel: The nanopillars are uncoupled. Their normalized propagation constant is equal to the effective index of the isolated waveguide, and the imprinted phase is independent of k_{\parallel} . Left panel: large spacings. Two supermodes are propagating and the imprinted phase that depends on both modes is not accurately controlled.

These considerations are general and may apply to other related devices [Lin14, Arb15]. Overall, Figure 3 summarizes the main design constraints and evidences the narrow working window for suitably selecting spacing – an essential parameter – and faithfully imprinting the desired phase profile. The narrow window led the present authors to choose a transparent material with a high-index (TiO_2 in the visible) to maximize the guiding effect by field confinement and to choose a spacing-to-wavelength ratio of 0.47 for the TiO_2 blazed-binary elements reported in Fig. 3. With this respect, it is instructive to compare this value with those of the blue, green and red metalenses reported in [Kho16], see Table 1.

The S/λ ratios of the blazed-binary elements and the blue metalens are almost identical, but the ratios used for the green and red metalenses are significantly larger. Using the rigorous-coupled-wave analysis, we have computed the supermodes of the nanopillar arrays at the blaze wavelengths for the three metalenses using the geometrical parameters given in the caption of Fig. 1 in [Kho16] and assuming that the array is periodic. We found that only the blue lens is designed with a spacing smaller than the structural cutoff, and that 3 and 4 supermodes, respectively, propagate in the green and red lenses. The consequence is that the phase imprinted in the green and red lenses is sensitive to small departures between the model and the actual component, and may vary as one varies the incidence angle or the wavelength. This is clearly seen in Fig. 1F in [Kho16], where the computed spectral

dependence of the metalens efficiencies is shown. The spectral responses of the green and red metalenses exhibit a rugged shape, whereas that of the blue lens that is designed with a spacing below the structural cutoff is perfectly smooth. This also explains why the efficiencies of the metalenses drops considerably as their operation wavelength increases from 405 to 660 nm, in opposition to the intuitive expectation that manufacturing difficulties disadvantage devices operating at small wavelengths. Another reason may be the difficulty encountered for fabricating nanostructured TiO_2 films with large thicknesses, so that the thicknesses for the green and red metalenses, which are the same and equal to the thickness of the blue metal lens, may not be large enough to implement the 2π discontinuity. This evidences the substantial technical achievement made during the fabrication of the blazed-binary elements for operation at 633 and 860 nm.

	Blazed binary elements [Lal99]	Metalenses [Kho16]		
Material	TiO_2	TiO_2		
Wavelength (nm)	633 – 860 nm	405 (blue)	532 (green)	660 (red)
Spacing S/λ	0.47	0.49	0.61	0.65
Efficiency	80%	86%	73%	66%
Polarization	Insensitive	Circular (cross)		

Table 1. Comparison between the blazed-binary gratings and lens manufactured in the 90's and the 2016 metalenses in [Kho16]. The phase encoding technique used for the metalens operates with circularly polarized light, whereas the technique in [Lal99] is polarization insensitive.

4.2 Efficiency

Large efficiencies, defined as the ratio between the power funneled into a specific desired order and the incident energy impinging on the diffractive element, are required for most applications. It is this efficiency that was considered in the previous figures and tables. It includes reflection losses. For imaging applications, it is acceptable that some power is lost by reflection, and another figure of merit, the relative efficiency defined as the fraction of the transmitted power that is effectively diffracted into the desired diffraction order, may be the proper parameter to maximize. Indeed, light that is not scattered into the desired diffraction orders feeds spurious diffractions orders (the diffraction orders of lens are the set of diverging or converging spherical waves with focal lengths that are integer sub-multiples of the nominal focal length) that deteriorate image quality by superimposing a coherent background.

In [Lal99, Lee02], substantial computations and optimizations were performed to evaluate what could be the best diffraction efficiencies achievable for blazed-binary diffractive elements with small zone widths (high NA) fabricated with TiO_2 pillars. Essentially, it was found that the relative efficiency slowly decreases from 100% for low NA to 85% for $NA = 0.5$. For larger NA 's, the zone width becomes comparable to the wavelength and resonance effects occur, producing chaotic unintuitive variations of the efficiency. Nevertheless, it was possible to design gratings with a deviation angle $\theta = 51^\circ$ ($NA = 0.8$) with a relative efficiency of 83% and to demonstrate experimentally a blazed-binary grating with a deviation $\theta = 40^\circ$ ($NA = 0.64$) and an efficiency of 80%. Further simulations have shown that, due to fabrication errors of the precise dimensions of the nanopillars and residual roughness, the measured efficiencies are 5-7% smaller than the theoretical values and $\approx 5\%$ smaller than the relative efficiencies. Similar figures hold for the off-axis 80%-efficient blazed-binary lens of Fig. 2c [Lal99].

To summarize, the possibility of implementing high-efficiency high- NA diffractive lenses with low absorption high-index material by implementing a guiding effect in the nanostructures has been known for almost 20 years, and the recent work at Harvard does not fundamentally change the situation, the green and red metalenses having even smaller efficiencies than those reported in earlier works. However with a 86% efficiency, the blue lens is remarkable, and it is interesting to understand it is slightly better than the blazed-binary diffractive elements. One possibility is a better fabrication technology. Another hypothesis is that polarization independence requires that the phase is varied by changing the size of the pillars. In total not all pillars are really independent from each other, especially tiny ones. In contrast, all pillars of the metalens are identical up to a rotation, and independence can be better satisfied.

4.3 Field of view

Commercial lenses for imaging applications are composed of several elements made from diverse materials, and some of their surfaces exhibit non-spherical shapes. This is required to correct for aberrations when imaging at wide angles and large fields with diffraction-limited focusing spots.

In sharp contrast, all metalenses fabricated up to now using the various approaches mentioned above use a single interface to imprint the phase. Single-interface lenses, whichever the method used for encoding the phase, have poor imaging capabilities. This is immediately realized by considering Fig. 4, which shows two focusing configurations at normal incidence (dashed blue) and at oblique incidence (solid red). Elementary geometrical calculations show that the phase-difference between points A and B that should be implemented for perfect focusing at normal incidence is $(\varphi_A - \varphi_B) = k_0(f^2 + r^2)^{1/2} - k_0f$, whereas it should be $k_0(f^2 + r^2)^{1/2} - k_0f + k_0r\theta \left(1 - (1 + (r^2/f^2))^{-1/2}\right)$ at small oblique incidence θ . Imposing that the phase deviation be smaller than 2π for aberration-free operation, we find that the field of view $FOV = 2f \tan(\theta)$ should be approximately smaller than

$$FOV < 4\lambda/NA^3. \quad [2]$$

For large NA , the field of view is very small, implying that single-interface lenses might be useful for point-to-point *interconnects* but not for high-performance imaging. Having this consideration in mind, it is inappropriate and even misleading to compare the imaging performance of a single-interface lens and multi-lens objectives corrected for aberrations, as done in [Kho16].

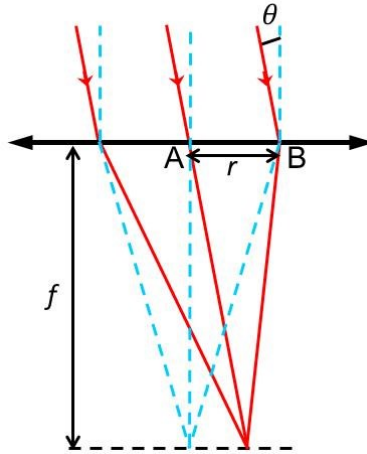


Fig. 4. Geometrical aberrations with single-surface imaging.

4.4 Broadband operation

The 2π -phase excursion is in general achieved at a single wavelength, the blaze wavelength used for the design. Illuminated at another wavelength, the 2π -phase excursion is not maintained and light is no longer funneled into a single order; the deviation results in the apparition of deterministic scattering into spurious diffraction orders, which represents a severe limitation for optical imaging systems designed to operate over finite spectral bands. Because the dispersion of most materials is weak away from their absorption bands, the efficiency dependence with the wavelength obeys a universal law $\eta = \text{sinc}^2(1 - \lambda_0/\lambda)$, λ_0 being the blazed wavelength for which the 2π -phase excursion is achieved [Swa89].

Metalenses bring a new degree of freedom. Because the artificial dielectric is much more dispersive than a bulk material, one should consider the dependence of the effective index with the wavelength, and the optical phase difference is now written

$$\frac{2\pi}{\lambda} \Delta = \frac{2\pi}{\lambda} (n(\lambda) - 1)t. \quad [3]$$

With this extra degree of freedom, it is possible to exploit the highly chromatic behavior of semiconductor structures with dimensions only slightly smaller than the wavelength to make the product $\frac{2\pi}{\lambda} (n(\lambda) - 1)$ nearly independent of wavelength. The idea was tested in [Rib13] with subwavelength structures consisting of a careful combination of micropillars and microholes. The device has been tested in the thermal infrared (band III) and blazing over nearly one octave was observed experimentally.

5. Conclusion

The previous analysis leads us to the following conclusive points:

- Focusing light with high-efficiency and high-NA is feasible at one wavelength in a point-to-point interconnection scheme with a single interface patterned with subwavelength high-index structures that guide light. This property that cannot be achieved with classical échelette diffractive optical elements is known since the late 90's [LaI99, La99a].
- High performance imaging (with high-NA) is not possible with a single diffractive (or refractive) interface, see [Section 4.3](#). Manufacturing high-efficiency and high-NA metolenses for high-

performance imaging requires to correct geometrical aberrations with several diffractive surfaces. It would be interesting to know what could be the minimum separation distance between the surfaces, but thinness and high performance imaging seems two incompatible objectives [Gis16].

- Broadband blazing (typically over one octave) with high relative efficiency has been demonstrated for applications in the thermal infrared with metasurfaces that exploit the highly chromatic behavior of subwavelength structures, see [Section 4.4](#). Unfortunately the demonstration uses holes, instead of pillars, in the shadow zone and since hole do not guide light efficiently, high efficiency is achieved only for devices with low deviation angles θ . There is no known metasurface designs that offer broadband blazing and high *NA*. Note that multilayer diffractive échelette-type components exist for broadband operation with ultra-high efficiency ($> 95\%$) and low-*NA* [Nak02]. Such components have been pioneered by Cannon in the EF 400mm f/4 DO IS USM teleobjective lens.
- Manufacturing cost matters. Échelette diffractive optical elements are presently manufactured at very low-cost in plastics essentially, with replication techniques such as roll-on, embossing ... [Gal97]. There is a common underlying cost to manufacturing metalenses. The latter require subwavelength features with large aspect ratios, see the last column in the Table of Fig. 2, making the fabrication not suitable for mass production. In this line of thought, fabrication constraints appear relaxed with metalenses implementing 2π -phase excursion with a combination of two resonances rather than with a propagation delay. The fabrication cost of metalenses based on plasmonic nanoantennas that may potentially be patterned on a low-cost flexible substrate with roll-on techniques could be markedly lower. However, in addition to efficiency issues, the low defect requirement needed to lower inevitable scattering due to roughness and impurities seems challenging.

Aside from those concerns on imaging issues with metalenses, niche applications may exist. Metasurfaces that provide fancy polarization behaviours with birefringent nanostructures, which cannot be easily implemented with classical refractive or échelette components, may offer new opportunities as recently demonstrated for single molecule spectroscopy for instance [Bac16].

References:

[Yu11] N. Yu, P. Genevet, M. A. Kats, F. Aieta, J.-P. Tetienne, F. Capasso, Z. Gaburro, Light propagation with phase discontinuities: generalized laws of reflection and refraction, *Science* **334**, 333–337 (2011).

[Kho16] M. Khorasaninejad, W. T. Chen, R. C. Devlin, J. Oh, A. Y. Zhu, F. Capasso, Metalenses at visible wavelengths: diffraction-limited focusing and subwavelength resolution imaging, *Science* **352**, 1190–1194 (2016).

[Swa89] G. J. Swanson, Binary optics technology: the theory and design of multilevel diffractive optical elements, *MIT Technical Report 854* (MIT, 1989).

[Aur72] L. d'Auria, J.-P. Huignard, A. M. Roy, E. Spitz, Photolithographic fabrication of thin film lenses, *Opt. Commun.* **5**, 232–235 (1972).

[Gal97] M.T. Gale, Replication techniques for diffractive optical elements, *Microelectr. Eng.* **34**, 321–339 (1997).

[Koc48] W.E. Kock, Metallic delay lenses, *Bell Syst. Tech. J.* **27**, 58–82 (1948).

[Sto91] W. Stork, N. Streibl, H. Haidner, P. Kipfer, Artificial distributed-index media fabricated by zero-order gratings, *Opt. Lett.* **16**, 1921–1923 (1991).

[Far92] W. M. Farn, Binary gratings with increased efficiency, *Appl. Opt.* **31**, 4453–4458 (1992).

[Kip94] P. Kipfer, M. Collischon, H. Haidner, J.T. Sheridan, J. Schwider, N. Streibl, J. Lindolf, Infrared optical components based on a microrelief structure, *Opt. Eng.* **33**, 79-84 (1994).

[Che95] F.T. Chen and H.G. Craighead, Diffractive phase elements on two-dimensional artificial dielectrics. *Opt. Lett.* **20**, 121-123 (1995).

[Zho95] Z. Zhou and T. J. Drabik, Optimized binary, phase-only, diffractive optical element with subwavelength features for 1.55 μm , *J. Opt. Soc. Am. A* **12**, 1104-1112 (1995).

[Mil96] J. M. Miller, N. de Beaucoudrey, P. Chavel, E. Cambril and H. Launois, Synthesis of Subwavelength Pulse Width Modulated Diffractive Optical Elements, *Opt. Lett.* **21**, 1399-1401 (1996).

[Che96] F.T. Chen and H.G. Craighead, Diffractive lens fabricated with mostly zeroth-order gratings, *Opt. Lett.* **21**, 177-179 (1996).

[War96] M.E. Warren, R.E. Smith, G.A. Vawter and J.R. Wendt, High-efficiency subwavelength diffractive optical element in GaAs for 975 nm, *Opt. Lett.* **20**, 1441-1443 (1996).

[Lal98] P. Lalanne, S. Astilean, P. Chavel, E. Cambril, H. Launois, Blazed-binary subwavelength gratings with efficiencies larger than those of conventional échelette gratings, *Opt. Lett.* **23**, 1081-1083 (1998).

[Lal99] P. Lalanne, S. Astilean, P. Chavel, E. Cambril, H. Launois, Design and fabrication of blazed-binary diffractive elements with sampling periods smaller than the structural cutoff, *J. Opt. Soc. Am. A* **16**, 1143-1156 (1999).

[Lee02] M.S.L. Lee, P. Lalanne, J.C. Rodier, P. Chavel, E. Cambril, Y. Chen, Imaging with blazed binary diffractive elements, *J. Opt. A.* **4**, S119-S122 (2002).

[La99a] P. Lalanne, Waveguiding in blazed binary diffractive elements, *J. Opt. Soc. Am. A* **16**, 2517-2520 (1999).

[Zei10] U.D. Zeitner, M. Oliva, F. Fuchs, D. Michaelis, T. Benkenstein, T. Harzendorf, E.B. Kley, High performance diffraction gratings made by e-beam lithography, *Appl. Phys. A – Mater. Sc. Eng.* **109**, 789-796 (2012).

[Hua13] L. Huang, X. Chen, B. Bai, Q. Tan, G. Jin, T. Zentgraf, and S. Zhang, Helicity dependent directional surface plasmon polariton excitation using a metasurface with interfacial phase discontinuity, *Light Sci. Appl.* **2**, e70 (2013).

[Che14] W.T. Chen, K.Y. Yang, C.M. Wang, Y.W. Huang, G. Sun, I.D. Chiang, C.Y. Liao, W.L. Hsu, H.T. Lin, S.L. Sun, L. Zhou, A.Q. Liu, D.P. Tsai, High-Efficiency Broadband Anomalous Reflection by Gradient Meta-Surfaces, *Nano Lett.* **14**, 225-230 (2014).

[Lin14] D. Lin, P. Fan, E. Hasman, M.L. Brongersma, Dielectric gradient metasurface optical elements, *Science* **345**, 298-302 (2014).

[Vo14] S. Vo, D. Fattal, W.V. Sorin, Z. Peng, T. Tran, M. Fiorentino, R.G. Beausoleil, Sub-wavelength grating lenses with a twist, *IEEE Photon. Technol. Lett.* **26**, 1375-78 (2014).

[Arb15] A. Arbabi, Y. Horie, A.J. Ball, M. Bagheri, A. Faraon, Subwavelength-thick lenses with high numerical apertures and large efficiency based on high-contrast transmitarrays, *Nature Commun.* **6**, 7069 (2015).

[Yu15] Y.F. Yu, A.Y. Zhu, R. Paniagua-Dominguez, Y.H. Fu, B. Luk'yanchuk, and A.I. Kuznetsov, High-transmission dielectric metasurface with 2π phase control at visible wavelengths, *Laser Photonics Rev.* **9**, 412-418 (2015).

[Rib13] C. Ribot, M.S.L. Lee, S. Collin, S. Bansropun, P. Plouhinec, D. Thenot, S. Cassette, B. Loiseaux, P. Lalanne, Broadband and efficient diffraction, *Adv. Opt. Mat.* **1**, 489-493 (2013).

[Gis16] T. Gissibl, S. Thiele, A. Herkommer and H. Giessen, Two-photon direct laser writing of ultracompact multi-lens objectives, *Nature Photonics* **10**, 554-560 (2016).

[Nak02] T. Nakai and H. Ogawa, Research on multi-layer diffractive optical elements and their application to camera lenses, in proceedings of the OSA Topical Meeting on Diffractive Optics and Micro-Optics, Tucson, Arizona (2002).

[Bac16] M.P. Backlund, A. Arbabi, P.N. Petrov, E. Arbabi, S. Saurabh, A. Faraon and W.E. Moerner, Removing orientation-induced localization biases in single-molecule microscopy using a broadband metasurface mask, *Nature Nanotechnology* **10**, 937–943 (2015).